Light Metals 2013 *Edited by: Barry Sadler*
TMS (The Minerals, Metals & Materials Society), 2013

INVESTIGATION OF ELECTROLYTIC BUBBLE BEHAVIOUR IN ALUMINUM SMELTING CELL

Morshed Alam[1], Yos Morsi[1], William Yang[2], Krishna Mohanarangam[2] Geoff Brooks[1] and John Chen[3]
[1]Faculty of Engineering and Industrial Sciences, Swinburne University of Technology, Hawthorn, Victoria, Australia.
[2]CSIRO Process Science and Engineering, Clayton, Victoria, Australia.
[3]Department of Chemical and Materials Engineering, University of Auckland, Auckland, New Zealand.

Keywords: Hall Heroult cell, Electrolytic process, Geometric and Dynamic Similarities.

Abstract

A 1/4th scale low temperature electrolytic model of the Hall-Heroult cell was constructed to investigate the electrolytic bubble formation mechanism, coalescence and movement under the horizontal anode surface. Geometric and dynamic similarity between the model and real cell was maintained through using similarity criteria. A 0.28M $CuSO_4$+20%H_2SO_4 solution was selected as an electrolyte where Cu was deposited at the cathode and O_2 bubbles were generated underneath the anode, similar to the phenomena of real cell. The bubble generation mechanism, movement, coalescence and detachment under the electrolytic medium were observed using a high speed camera. It was found that electrolytic bubbles generate uniformly under the whole anode surface and grow through gas diffusion and coalescence. At higher current density and higher anode inclination angles, bubbles escape quickly from underneath the anode surface. The bubble layer thickness and bubble sizes were also found to decrease with an increase in anode inclination angle.

Introduction

Aluminum is produced by Hall-Heroult electrolytic process which was invented independently by Hall and Heroult in 1886. In this method, alumina (Al_2O_3) is dissolved in a molten cryolite (Na_3AlF_6) bath at around 950^0C where it is reduced to produce liquid aluminum metal and oxygen ions. The liquid aluminum metal is slightly denser than the electrolyte and is continuously deposited at the bottom of the cell while the oxygen reacts with the carbon anode to form CO_2. The overall cell reaction is:

$$2Al_2O_{3(solution)} + 3C_{(s)} = 4Al_{(l)} + 3CO_{2(g)} \quad (1)$$

The gas bubbles induce flow in the cell which plays an important positive role in homogenization of the alumina distribution and the temperature field in the electrolytic bath. Conversely, the gas bubbles increase the ohmic voltage drop underneath the anode surface which in turn results in higher energy consumption for the smelting process. The phenomenon of bubble formation and sliding underneath the horizontal surface is complex due to the bubble shape, surface tension and the anode surface characteristics. A number of studies have been carried out in the past on the bubble behavior under the anode surface and its effect on the electrolyte flow. Fortin et al.[1] used a full-scale water model where anodic gas evolution was simulated by passing air through a micro-porous polyethylene plate. The flow rate of air was selected from the current density and gas evolution correlation (four electrons are necessary to produce one mole of CO_2) which is 10 kAm^{-2} = 2.71 $Lm^{-2}s^{-1}$. The gas bubbles nucleate at the porous sections on the anode surface and undergo spherical growth, lateral spread, mutual impingement and coalescence to form a big bubble as shown schematically in Figure 1. The bubbles are then roll along the anode surface and escape around the anode edge. The measured gas bubble layer thickness was approximately 5mm for a horizontal anode. The effects of current density (CD), anode-cathode distance (ACD) and anode inclination angle on the gas layer geometry, anode coverage, bubble velocity and gas release frequency were investigated. ACD had no effect on gas bubble behavior. An increase in CD increased the bubble size, thickness of bubble front, average fraction of anode surface covered by bubbles and the bubble velocity while an inclined anode was found to decrease these parameters. The bubble release frequency was found to vary from 0.2 to 3.3 Hz depending on the anode inclination angle and was not influenced by the CD.

Figure 1 Bubble shape according to Fortin et al.[1]

Solheim and Thonstad [2] found that bubble size decreased with the addition of i-propanol which inhibits the coalescence. It was reported that the smaller bubble size results in higher accumulated gas volume as well as higher resistivity in the bubble layer. Shekhar and Evans [3] observed that the bubble layer becomes thinner in the case of a tilted anode. Xiang-peng et al. [4] reported that the bubble detachment volume decreases and bubble sliding velocity increases with an increase in anode inclination angle. The bubble velocity was found to decrease when ACD was less than 4cm which is in contrast with the results of Fortin et al. [1] where it was reported that ACD has no effect on bubble behavior. Che et al. [5] observed that the bubble shape changes from ellipsoid to crescent with an increase in gas flow rates. In a later studies, Perron et al. [6] observed the existence of two distinct bubble regimes under the anode surface: "creeping bubble (a and b)" and "the bubble on a wetting film (c and d)" as shown in Figure 2.

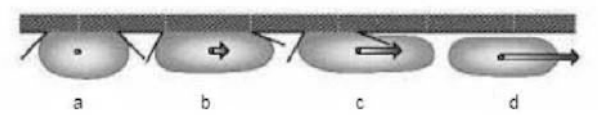

Figure 2 Regimes of movement of the bubbles[6].

Aussilllous and Quere [7] also reported the formation of a liquid film between the bubble and anode surface. During creeping motion, the longer axis lies in the direction of the displacement while for wetting film bubbles the longer axis lies perpendicular to the displacement.

Das et al. [8] observed that bubbles lose their symmetric shape immediately after the detachment when sidewall is at a close proximity. In their other studies [9, 10], it was reported that bubble size increases with an increase in liquid surface tension and decreases at higher anode inclination angle.

Cooksey and Yang [11, 12] measured bubble induced liquid flow in a full scale water model of aluminum reduction cell using Particle Image Velocimetry (PIV) technique. A recirculation zone was detected in both the center and side channel of the cell. The area of high turbulence was located in the gas plume region near the end of the anode and at the liquid surface. Wang et al. [13] observed similar phenomenon using the Laser Dopler Velocimetry (LDV) technique in their physical modeling study.

In the physical modeling studies that have been discussed so far, gas bubbles were generated mechanically by injecting air underneath the anode surface. Qian et al. [14, 15] pointed out from their low temperature electrolytic model that electrolytically generated bubbles are smaller compared with the bubbles formed by forcing air through porous plate. 2M NaOH was used as electrolyte in their study and the anode surface was covered with foamy layer of tiny bubbles. It was found that at equal current density or equivalent gas generation ratio, bubble resistivity was 20% higher in case of electrolytically generated bubbles.

There have been a number of studies [16-20] using bench-scale experiments where bubbles were generated electrolytically and the electrochemical reactions are similar to those in an actual cell. However, in those studies the anode surface area was too small (10-20mm) compared with the actual cells except the one of Aaberg et al. [21]. As a result, the measured bubble sizes may be different as it is known from the physical modeling that bubbles coalesce during movement under the horizontal anode. Aaberg et al. [21] carried out bench-scale experiments of real aluminum electrolytic cell using a 100mm graphite anode. The average bubble volume at release, bubble thickness and fraction of anode surface covered by anode were reported. However, it is very difficult to make visual observation of the electrolytic bubble formation, coalescence and growth mechanism due to the opaque electrolytic bath of bench-scale experiments. Therefore, the aim of this work was to enhance the current understanding of the electrolytic bubble formation, movement and detachment characteristics, under the horizontal anode surface, using a low temperature electrolytic model of the Hall-Heroult Cell.

Design of Electrolytic Cell

In designing the low temperature electrolytic model, emphasis was on maintaining the geometric and dynamic similarity between the real cell and the low temperature electrolytic model. A 1/4th scale model of the Hall-Heroult cell was built by maintaining complete geometric similarity. In order to maintain the dynamic similarity, five different dimensionless numbers were considered as reported by Zhang et al. [22]. These are

Modified Froude number = (Inertial force)/(Buoyancy force) $=(\rho_g q^2)/(\rho_l-\rho_g)gL$

Modified Weber number = (Inertial force)/(Surface tension force) $=(\rho_g q^2 L)/\sigma$

Modified Reynolds number = (Inertial force)/(Viscous force) $=(\sqrt{(\rho_l \rho_g)}qL)/\mu$

Eotvos number = (Buoyancy force)/(Surface tension force) $=(g(\rho_l-\rho_g)L^2)/\sigma$

Morton number = $(g\mu_l^4(\rho_l-\rho_g))/(\rho_l^2\sigma^3)$

Here, q is the gas generation rate per unit surface area, g is the acceleration due to gravity, ρ_l is the liquid density, ρ_g is the gas density and σ is the surface tension of surrounding liquid, L is the characteristic dimension and μ_l is the viscosity of surrounding liquid.

From the literature review, it can be concluded that the buoyancy force and inertial force generated by the evolving gases are the main driving forces for the bubble movement and bath motion. Also, the Eotvos number together with Morton number is used to characterize the bubble size and shape moving in a surrounding fluid medium. Hence, in the present study, the Modified Froude number, Eotvos number and Morton number were considered for dynamic similarity analysis and are presented in Table 1:

Table 1: Fluid properties and dynamic similarity analysis of the present model

	Real Cell	Present model
Electrolyte	Cryolite	0.28M $CuSO_4$+20%H_2SO_4
Electrolyte density (kg/m^3)	2100	1195[23]
Electrolyte surface tension (mN/m)	129	98.7[24]
Electrolyte viscosity (kg/ms)	0.00251	0.0011[23]
Bubble cross section diameter before release, (mm)	11 - 13[18, 19]	5 - 18
Anode length, (m)	1.35[1]	0.35
Modified Froude number	1.162×10^{-10}	1.43×10^{-11}
Eotvos number	19.32 - 27	2.97 – 38.4
Morton number	8.6372×10^{-11}	1.245×10^{-11}

Table 1 shows that the Eotvos number and the Morton number of the model and real cell have similar order of magnitude. Hence, it can be said that the generated bubble shape in the model cell is likely to be similar to that of a real cell because these dimensionless numbers characterize the shape of bubbles. The bubble cross-section diameter before release was used as the characteristic dimension in the Eotvos number equation. Table 1 also shows that Modified Froude number of the real cell is one order of magnitude higher than the model cell. This was because the gas generation rate in the present model cell was lower than the desired value. An increase in current density increases the

bubble release frequency, but the bubble volume at release is not influenced by the current density [21]. The main goal in this experiment was to generate bubbles electrolytically which are comparable with the bubbles of real Hall-Heroult cell and then study the bubble formation, movement and detachment under the horizontal anode. That is why emphasis was given on the Eotvos number and Morton number as these numbers characterize the bubble shapes.

Experimental rig

In the previous low temperature electrolytic study of Qian et al.[14], 2M NaOH was used as the electrolyte, so bubbles generate both at the cathode and anode. But in the actual cell, no bubbles are generated at the cathode. Therefore, a separator was used to isolate the bubbles that generated at the cathode in order to minimize the effect of cathode bubbles on the anode. In the present study, the electrolyte was selected in such a way that no bubbles should generate at the cathode. After studying the available aqueous solutions, it was found that $CuSO_4$ solution is an excellent candidate, and therefore was used in this study. The overall electrolytic reaction is:

$$CuSO_4(aq) + 2e^- + H_20 = Cu(s) + H_2SO_4(aq) + \tfrac{1}{2} O_2(g) \quad (2)$$

Figure 3 shows the experimental set-up used in the present study. The inside dimensions of the model cell was 500mm x 115mm x

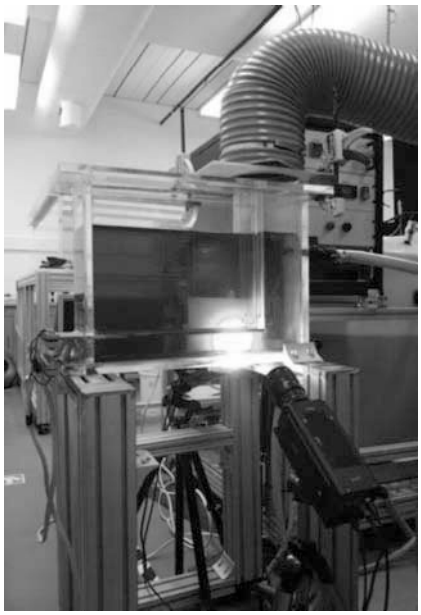

Figure 3 Experimental set-up.

400mm. The anode and cathode dimensions were 350mm x 115mm and were placed parallel to each other. These dimensions were decided according to 1/4th scale geometrical similarity analysis with the real cell[1]. The ACD was fixed at 50mm. Lead and stainless steel plates were used as the anode and cathode respectively. The anode immersion depth was fixed at 200mm. The $CuSO_4$ solution was stored in a tank where it was heated and maintained at 50^0C. The electrolyte was supplied into the model cell through the inlet at the bottom left corner of the cell. When the electrolyte level reached 250mm from the bottom, it passed through the electrolyte overflow line into the heated tank from where it was recirculated again into the cell. A DC power supply (0- 500A) was used to supply current for electrolysis. But current could not be increased over 125A as the voltage drop was greater than 5V which is the maximum voltage reading for this power supply unit. In the electrolytic process, the oxygen bubbles create acid mist at the liquid surface which is hazardous for human health. A 200mm flexible reinforced PVC pipe was placed on top of the cell to extract the generated acid mist as shown in Figure 3.

Experimental Procedure

The electrolyte (0.28M $CuSO_4$ + 20% H_2SO_4) was circulated continuously from the heated tank to the experimental rig to ensure that the temperature of the electrolyte remained around 45-50^0C inside the model cell, which is the requirement for the electrolysis of $CuSO_4$ solution. The temperature was monitored through a digital stem thermometer (accuracy $\pm 0.10^0$C). The circulation was turned off prior to the commencement of electrolysis so that the liquid velocity did not affect the bubble behavior. Then, the power supply was turned on and set to the desired current density to commence the electrolysis. The experiments were run at different current densities and anode inclination angles to investigate the effect of these parameters on the bubble characteristics. The operating conditions used are presented in Table 2:

Table 2 Operating Conditions.

Experiment no	Angle of inclination (degree)	Current density (A/cm^2)	Calculated gas generation rate ($m^3m^{-2}s^{-1}$)$\times 10^{-3}$
1	1	0.074	0.051
2	1	0.087	0.06
3	1	0.1	0.068
4	1	0.112	0.077
5	2	0.074	0.051
6	2	0.087	0.06
7	2	0.1	0.068
8	2	0.112	0.077
9	3	0.074	0.051
10	3	0.087	0.06
11	3	0.1	0.068
12	3	0.112	0.077
13	3	0.31	0.213

The average bubble cross-sectional diameter and thickness (l and d in Figure 7 respectively) of the departing bubbles from the edge of the anode surface were measured using the high speed camera at 250 frames per second from two different locations: (a) perpendicular to the direction of motion of the bubbles and (b) inclined from the horizontal plane. The captured images were then processed using image processing software "imageJ".

Results and Discussions

After the start of electrolytic process, the entire underside of the anode was covered by tiny bubbles as shown in Figure 4. Gradually the immobile bubbles grew in size due to gas diffusion and then through coalescence with the surrounding bubbles. There were no clear areas under the anode as compared to water modeling studies [1, 13, 25]. The bubbles remained stationary

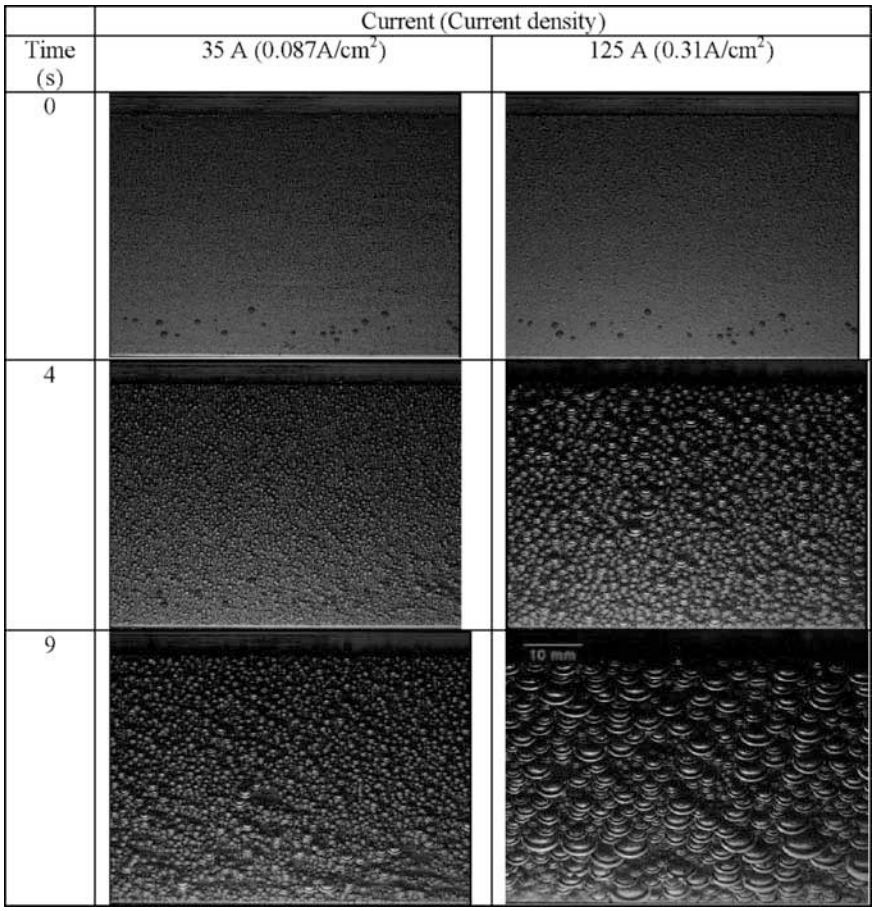

Figure 4 Initial bubble formation under the anode surface at 0.087 A/cm^2 and 0.31 A/cm^2 current density and 1 degree angle.

at the nucleation point until the component of the buoyancy force, parallel to the anode surface, was large enough to overcome the surface tension force and drag force. This occurred when the bubbles reached a certain volume at a constant angle. After that the bubbles detached from the nucleation site and slide along the anode surface. Bubble size before detachment also depends on the anode inclination angle which will be shown later in this paper. The formation and movement mechanism was similar at both higher and lower current densities. The higher current density only speeds up the process as shown in Figure 4. At t=4 sec, the bubbles started to detach from the nucleation point in case of 0.31A/cm^2 current density whereas the bubbles were only growing in case of 0.087A/cm^2 current density. These figures also show that although small bubbles generated under the entire anode surface, the bubbles grew bigger only at a limited number of nucleation sites, which may depend on the morphology of the anode surface. A separate study on this particular issue is required to understand the effect of anode properties on bubble characteristics.

Figure 5 shows the bubble flow pattern under the anode surface at different anode angles and at a fixed current density of 0.112A/cm^2. A number of larger bubbles were observed when the anode was 1 degree, and bubble sizes decreased at higher inclination angles. At the beginning of electrolysis, the shape of the bubbles (less than 4mm) were spherical and then slowly

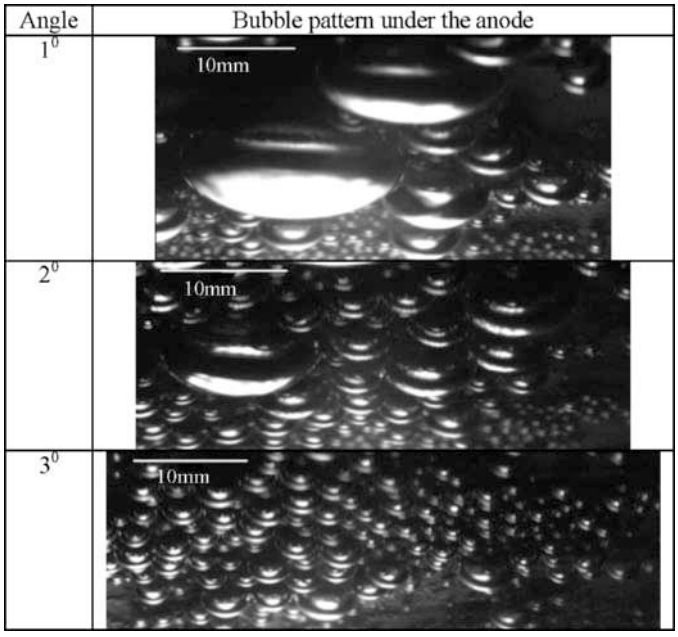

Figure 5 Bubble pattern under the electrode at different anode angle and 0.112A/cm^2 CD.

converted to ellipsoid as these grew bigger due to coalescence. Figure 6 shows that the cross-section diameter of the detached bubble decreases with an increase in anode inclination angle. This occurred because at higher inclination angle bubbles were travelling faster and didn't get enough time to coalesce. When the anode was nearly horizontal (1 degree), the measured mean bubble cross-section diameter was 10.76mm with a standard deviation of ±4.47mm. This value is lower than the reported value of 18mm by Cassayre et al. [19] at similar current density. The reason for the difference might be that the anode was perfectly horizontal in the previous study[19] whereas in our case the anode angle was 1 degree. But the present results agreed well with the results of Xue and Oye [18] which ranged from 11-12mm at practical current density of smelting cell.

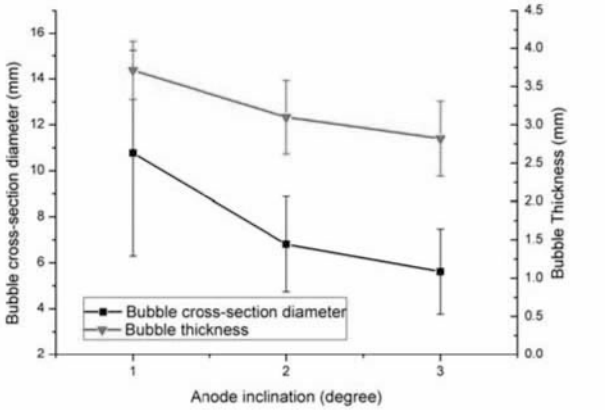

Figure 6 Average bubble diameter and thickness under anode before release. Current density is 0.112A/cm^2.

The thickness of the gas bubble layer under the anode surface reached a maximum of 4.1mm with an average of 3.71mm in case of 1 degree anode inclination angle. This is in good agreement with reported maximum thickness of 4mm and 5mm from the previous laboratory scale aluminum electrolysis studies [17, 18, 21] . The thickness of the gas film was also found to decrease with an increase in anode inclination angle as shown in Figure 8, which was also observed by Shekhar and Evans [3] in their physical modeling study. This was expected because at higher inclination angle, the gas bubble velocity increases and the gas film thickness should decrease to satisfy the continuity equation.

Wettability is an important parameter for investigating the bubble characteristics underneath the anode surface. The notion of wettability is based on the concept of an equilibrium state between the interfacial surface tension of three phases and the existence of equilibrium contact angle. The contact angle is the angle between the solid surface and the gas-liquid interface as shown in Figure 7. The final contact angle of the bubble with the anode surface before departure was measured using the image analysis software "imageJ". The measured bubble contact angle was found to vary from 115 degree to 135 degree which are in good agreement with the results of Xue and Oye [18] that ranged from 110 to 130 degree.

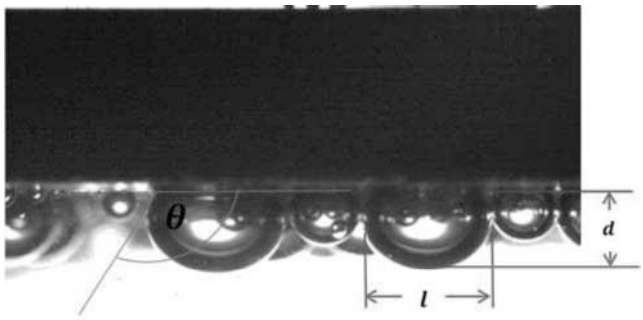

Figure 7 Bubble contact angle under anode surface

Figure 8 shows the change in bubble terminal velocity before detachment from the anode surface with increasing current density. As expected, the bubble terminal velocity was found to increase with the increase in current density. This occurs because, at higher current density, the bubble generation rate increases underneath the anode surface. As the bubble penetration depth inside the electrolyte is limited, more and more bubbles slide under the anode surface and escape through the anode edge at higher velocity if the current density is increased. The figure also shows that bubble terminal velocity increases with the increase of electrode inclination angle. The component of the buoyancy force parallel to the anode plane increases at higher inclination angle which in turn accelerates the gas bubbles underneath the anode surface and the bubbles escape quickly from the edge of the anode.

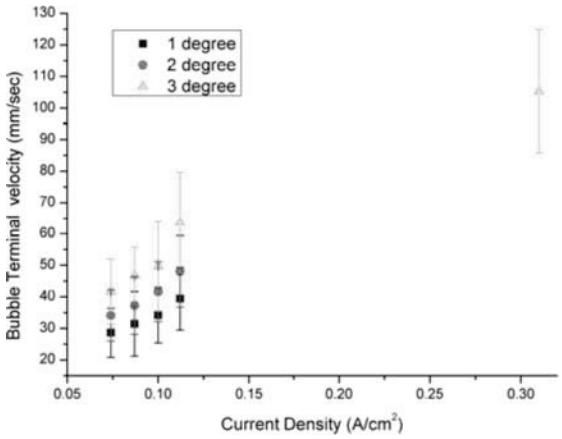

Figure 8 Effect of current density on bubble terminal velocity.

Conclusions

A 1/4th scale low temperature electrolytic model of the Hall-Heroult cell was developed to investigate the bubble characteristics under the anode surface. 0.28M$CuSO_4$ + 20%H_2SO_4 solution was used as electrolyte which deposited Cu at cathode and produced O_2 bubbles under the anode during electrolysis. Proper Similarity analysis was carried out to make the model geometrically and dynamically similar with the real cell. The behaviour of the electrolytically generated bubbles were analysed through high speed camera. It was observed that electrolytic bubbles generate uniformly under the anode surface

and then grow bigger due to gas diffusion and coalescence. The average bubble size before detachment from the anode edge and thickness was found to be 10.76mm and 3.7mm when the anode was nearly horizontal. These values were close to previous literature predictions. The bubble size decreased and bubble terminal velocity increased with an increase in anode inclination angle. The bubble terminal velocity was also found to increase with an increase in current density. The observed contact angle between anode and the gas bubbles was ranging from 115 to 135 degrees which was also in good agreement with the previous studies. At present, this study is going on to investigate the effect of anode angle and current density on the anode coverage ratio, bubble resistance and bubble volume before detachment. The results will be presented in future publications.

Acknowledgments

Authors would like to acknowledge CSIRO Light Metals Flagship, Australia for funding the project.

References

1. Fortin, S., Gerhardt, M., and Gesing, A.J., Physical Modelling of bubble behaviour and gas release from aluminium reduction cell. in *Light Metals*. 1984. TMS: p. 721-741.
2. Solheim, A. and Thonstad, J., Model Cell Studies of Gas Induced Resistance in Hall-Heroult Cells. in *Light Metals*. 1986. TMS: p. 397-403.
3. SHEKHAR, R. and EVANS, J.W., Physical Modelling Studies of Electrolyte Flow Due to Gas Evolution ans Some Aspects of Bubble Behaviour in Advanced Hall Cells: Part 1. Flow in Cells With a Flat Anode. *Mtallurgical and Materials Transactions B*, 1994. **25**(June): p. 333-340.
4. Xiang-peng, L., Jie, L., Yan-qing, L., Heng-qin, Z., and Ye-xiang, L., Physical modelling of gas induced bath flow in drained aluminium reduction cell. *Trans. Nonferrous Met. Soc. China*, 2004. **14**(5): p. 1017-1022.
5. Che, D.F., Chen, J.J.J., and Taylor, M.P., *Gas Bubble Formation And Rising Velocity Beneth a Downward Facing Inclined Surface Submerged in a Liquid*, in *18th Australiatian Chemical Engineering Conference*1990, CHEMECA: Auckland. p. 384-391.
6. Perron, A., Kiss, L.I., and Poncsak, S., Regimes of the Movement of Bubbles Under the Anode in an Aluminium Electrolysis Cell. in *Light Metals*. 2005. TMS: p. 565-570.
7. Aussillous, P. and Quere, D., Bubbles creeping in viscous liquid along a slightly inclined plane. *Europhysics letters*, 2002. **59**(3): p. 370-376.
8. Das, S., Morsi, Y., Brooks, G., Yang, W., and Chen, J.J.J., Experimental investigation of single bubble characteristics in a cold model of a Hall Héroult electrolytic cell. in *Light Metals*. 2011. TMS: p. 575-580.
9. Das, S., Morsi, Y., Brooks, G., Yang, W., and Chen, J.J.J., Principal characteristics of a bubble formation on a horizontal downward facing surface. *Colloids and Surfaces A: Physicochemical and Engineering Aspects*, 2012. **411**: p. 94-104.
10. Das, S., Morsi, Y., Brooks, G., Yang, W., and Chen, J.J.J., *The Principle characteristics of the detachment and sliding mechanism of gas bubbles under an inclined anode*, in *10th Australian aluminium smelting technology conference*9-14 October, 2011: Launceston.
11. Cooksey, M.A. and Yang, W., PIV Measurement of Physical Models of Aluminium reduction cells. in *Light Metals*. 2006. TMS: p. 359-365.
12. Yang, W. and Cooksey, M.A., Effect of slot height and width on liquid flow in physical models of aluminium reduction cells. in *Light Metals*. 2007. TMS: p. 451-456.
13. Wang, Y., Zhang, L., and Zuo, X., Fluid Flow and Bubble Behaviour in The Aluminium Electrolysis Cell. in *Light Metals*. 2009. TMS: p. 581-586.
14. Qian, K., Chen, J.J.J., and Matheou, N., Visual observation of bubbles at horizontal electrodes and resistance measurements on vertical electrodes. *Journal of Applied Electrochemistry*, 1997. **27**: p. 434-440.
15. Qian, K., Chen, Z.D., and Chen, J.J.J., Bubble Coverage and Bubble Resistance using cells with horizontal anode. *Journal of Applied Electrochemistry*, 1998. **28**: p. 1141-1145.
16. Dorin, R. and Frazer, E.J., Operational Characteristics of Laboratory Scale Alumina reduction cells with wettable cathodes. *Journal of Applied Electrochemistry*, 1993. **23**: p. 933-942.
17. Utigard, U., Costa, J.H., Popelar, P., Walker, D.I., Cool, G., and Hoang, P., Visualization of the Hall-Heroult Process. in *Light Metals*. 1994. TMS: p. 233-240.
18. Xue, J. and Oye, H.A., Bubble Behaivour-Cell Voltage Oscillation during aluminium electrolysis and the effects of sound and ultrasound. in *Light Metals*. 1995. TMS: p. 265-271.
19. Cassayre, L., Torstein, A., Utigard, U., and Bouvet, S., Visualizing gas evolution on graphite and oxygen-evolving anodes. *JOM*, 2002: p. 41-45.
20. Wang, X. and Tabereaux, T., Anodic Phenomena-Observations of Anode Overvoltage and Gas Bubbling During Aluminium Electrolysis. in *Light Metals*. 2000. TMS: p. 239-247.
21. Aaberg, R.J., Ranum, V., Williamson, K., and Welch, B.J., The Gas Under Anodes in Aluminium Smelting Cells Part 2: Gas Voumes and Bubble Layer Characteristics. in *Light Metals*. 1997. TMS: p. 341-346.
22. Zhang, W.D., Chen, J.J.J., and Taylor, M.P., Similarity Analysis of Gas Induced Bath Flow in Hall-Heroult Cells. in *CHEMECA*. 1990. Auckland: p. 1-8.
23. Price, D.C. and Davenport, W.G., Densities, Electrical Conductivies and Viscosities of $CuSO_4$/H2SO4 Solutions in the Range of Modern Electrorefining and Electrowinning Electrolysis. *Metallurgical and Materials Transactions B*, 1980. **11**: p. 159-163.
24. Djokić, S.S., *Electrodeposition: Theory and Practice*2010, New York: Springer. 57.
25. Zoric, J. and Solheim, A., On gas bubbles in Industrial aluminium cells with prebaked anodes and their incluences on current distribution. *Journal of Applied Electrochemistry*, 2000. **30**: p. 787-794.